Journal of Power Sources 261 (2014) 255–263

Contents lists available at ScienceDirect

Journal of Power Sources

journal homepage: www.elsevier.com/locate/jpowsour

Evaluation of Li_2O as an efficient sintering aid for gadolinia-doped ceria electrolyte for solid oxide fuel cells

Tenglong Zhu [a,1], Ye Lin [b,1], Zhibin Yang [a], Dong Su [c], Shuguo Ma [d], Minfang Han [a,*], Fanglin Chen [b,*]

[a] Union Research Center of Fuel Cell, China University of Mining & Technology, Beijing 100083, China
[b] Department of Mechanical Engineering, University of South Carolina, Columbia, SC 29208, USA
[c] Center for Functional Nanomaterials, Brookhaven National Laboratory, Upton, NY 11973, USA
[d] College of Engineering and Computing, University of South Carolina, Columbia, SC 29208, USA

HIGHLIGHTS

- Using Li_2O as sintering aid, gadolinia-doped ceria (GDC) be densified at 900 °C.
- Surface and bulk morphology of the sintered GDC samples was evaluated.
- Li-containing residues in the sintered GDC samples were examined.
- Bulk conductivity of 0.059 S cm^{-1} at 600 °C was achieved for GDC sintered at 1000 °C.

ARTICLE INFO

Article history:
Received 17 December 2013
Received in revised form
2 March 2014
Accepted 5 March 2014
Available online 24 March 2014

Keywords:
Gadolinia-doped ceria
Sintering aid
Conductivity
Electrolyte
Solid oxide fuel cell

ABSTRACT

Li_2O has been evaluated as a sintering aid for $Gd_{0.1}Ce_{0.9}O_{2-\delta}$ (GDC). Using 2.5 mol% ratio of Li_2O to GDC (5LiGDC), dense samples with relative density of 99.3% were achieved at sintering temperature as low as 900 °C. A high total conductivity of 0.059 S cm^{-1} at 600 °C was obtained for the 5LiGDC samples sintered at 1000 °C (5LiGDC1000), while 5LiGDC samples sintered at 1400 °C showed a lower conductivity of 0.017 S cm^{-1} at 600 °C. It has been found that Li_2O has the tendency to accumulate in the grain boundary region to form Li–Gd–Ce–O phases when the 5LiGDC sintering temperature is at 1000 °C or below, leading to an increase in the grain boundary conductivity. Increasing the 5LiGDC sintering temperature above 1000 °C will accelerate the vaporization of Li_2O, association of the oxygen vacancy and formation of additional pores in the bulk, resulting in a decrease of both the grain boundary and grain interior conductivity. Secondary ion mass spectrometry (SIMS) results have confirmed the existence of Li ions for the 5LiGDC samples sintered at or below 1000 °C, while most of Li species has vaporized for the 5LiGDC samples sintered above 1000 °C.

1. Introduction

Solid oxide fuel cell (SOFC) is an energy conversion device that can convert the chemical energy of the fuel directly to electricity with high efficiency, low emissions and fuel flexibility, and has recently attracted significant attentions worldwide due to the limited fossil fuel resources and the increasing environmental concerns [1]. Electrolytes for SOFCs are mainly based on the yttrium doped zirconia (YSZ) and gadolinium doped ceria (GDC), of which GDC possesses much higher conductivity at lower operating temperatures [2–4]. Consequently, GDC has been expected to be an ideal electrolyte operating at low operating temperatures of 400–600 °C [5–8]. However, high sintering temperatures such as 1550 °C are typically needed to densify GDC electrolyte [9], increasing cost and difficulty in the cell fabrication process. Consequently, lowering the sintering temperature to achieve relatively high density of sintered GDC samples has become an active research area. Two main approaches have been extensively explored to enhance the sinterability of GDC. The first one is to use different powder preparation methods such as co-precipitation and hydrothermal method to synthesize active nano-sized GDC powders with high sintering ability [10–12]. However, the complex powder synthesis process and low yield make it difficult for cost

* Corresponding authors. Tel.: +1 803 777 4875; fax: +1 803 777 0106.
E-mail addresses: hanminfang@sina.com (M. Han), chenfa@cec.sc.edu (F. Chen).
[1] These authors contributed equally to this work.

http://dx.doi.org/10.1016/j.jpowsour.2014.03.010
0378-7753/

effective and scalable practical applications. Another strategy is to apply sintering aid to reduce the sintering temperature. Jud et al. [13] successfully lowered the sintering temperature by 200 °C using 1 mol % ratio of cobalt oxide as the sintering aid to GDC, while Perez-Coll and co-workers [14] found that the addition of Co_3O_4 lowered the grain and grain boundary activation energy, and at the same time increased the grain and grain boundary conductivity in lower temperature zone.

In our previous study [15], 2.5 mol % Li_2O was applied as the sintering aid for GDC (5LiGDC) and dense GDC samples has been obtained at a low sintering temperature of 800 °C. For application of GDC as the electrolyte in SOFCs, the conductivity value of GDC is one of the most important metrics that should be evaluated. The total conductivity could be further separated into the grain interior conductivity and grain boundary conductivity, and both of them could be influenced when using Li_2O as the sintering aid. On the other hand, easy vaporization of Li_2O at high temperatures makes it even more complicated for the sintering processes [16]. The objective of this study is to examine the conductivity of 5LiGDC samples sintered at different temperatures, to characterize the composition and microstructure of the sintered samples, to study the shrinkage behavior of the samples during sintering, and to elucidate possible sintering mechanisms.

2. Experimental

$Gd_{0.1}Ce_{0.9}O_{2-\delta}$ (GDC) raw powder was synthesized from a sol–gel method [17]. Specifically, $Ce(NO_3)_3{\cdot}6H_2O$ and Gd_2O_3 were mixed in stoichiometric ratio and ball milled for 48 h. 5 wt% of $(NH_4)_2SO_4$ was then added as initiator and 2 wt% of *N*,*N*,*N*′,*N*′-tetramethylethylenediamine as the catalyst. The mixture was stirred until a sol–gel was formed. The sol–gel was then dried and calcined at 800 °C for 2 h to obtain the GDC powder. 5 mol% ratio of $LiNO_3$ was added into GDC (5LiGDC) (equals to 2.5 mol% Li_2O doped GDC since $LiNO_3$ will decompose to Li_2O at 600 °C) with ethanol as dispersant and ball milled for 24 h. The slurry containing $LiNO_3$ and GDC was dried at 65 °C and the mixture obtained was further calcined at 600 °C for 2 h. The 5LiGDC powder was then die-pressed (220 MPa) to pellets with diameter of 20 mm and thickness of 0.8 mm. The 5LiGDC pellets were firstly heated up at a heating rate of 3 °C min^{-1} to 600 °C for 2 h, then further sintered at 900, 1000, 1100, 1250 and 1400 °C for 6 h with a heating rate of 1 °C min^{-1}, and finally cooled down to room temperature. The sintered pellets were noted as 5LiGDC900, 5LiGDC1000, 5LiGDC1100, 5LiGDC1250 and 5LiGDC1400, respectively. Relative densities were all above 95% for the sintered pellets tested by the Archimedes drainage method. For comparison, GDC pellets without adding Li_2O were also sintered at 1400 °C (denoted as GDC1400). The surface of all the pellets was polished using 600 grid sand paper prior to the conductivity tests.

The phases of the sintered samples were characterized using X-ray diffractometer (XRD, PANalytical, X'PertPRO, the Netherlands) with CuKα radiation, a scanning step of 0.02°, a scanning speed of 3° min^{-1}, and 2θ range of 10–90°. Netzsch Dil402C dilatometer was used to study the sintering behavior of the 5LiGDC and GDC samples in air, with a heating rate of 10 °C min^{-1} up to 1400 °C. In order to exclude the surface adsorption impurity elements influence, the sintered samples were polished and thermally etched for surface microstructure study using scanning electron microscope (SEM, JEOL JSM 6700F and Zeiss Ultraplus). The cross section images were taken from samples without thermal etching as to keep the origin status. transmission electron microscopy (TEM) samples were prepared by classic dimpling method using the Gatan dimpler 626, and the final sample thickness was down to <10 nm by ion milling (Fischione Model 1010) .The local elemental distributions are characterized by the scanning transmission electron microscope with energy-dispersive X-ray spectroscopy (STEM-EDX) method using a Cs-corrected Hitachi HD-2700C equipped with a Cold-FEG, operated at 200 kV. Secondary ion mass spectrometry (SIMS, Hiden Analytical Ltd.) is also utilized as a complementary surface analytical method to XRD and SEM. For SIMS tests, Ar^+ primary ions accelerated in the range of 5 keV are bombarded to the surfaces of the samples. A small fraction of the samples is evaporated from the outer surface layer, producing various different kinds of ionized molecular fragments. The ionized molecular fragments are counted using a quadrupole mass spectrometer. The mass of the fragments provides information on the chemical species formed on the samples uppermost surface layers.

Ag electrodes (with diameter of ~0.8 cm) were coated on both sides of the dense pellets and fired at 700 °C for 0.5 h. Electrochemical impedance spectroscopy measurements were performed using a Zahner IM6 Electrochemical Workstation under dry air in a temperature range between 150 and 700 °C over the frequency range of 0.1 Hz to 4 MHz.

3. Results and discussion

3.1. Structural analysis

Fig. 1 shows the XRD of 5LiGDC pellets sintered at different temperatures (900, 1000, 1100, 1250 and 1400 °C, respectively) and GDC pellets sintered at 1400 °C, respectively. The same sample

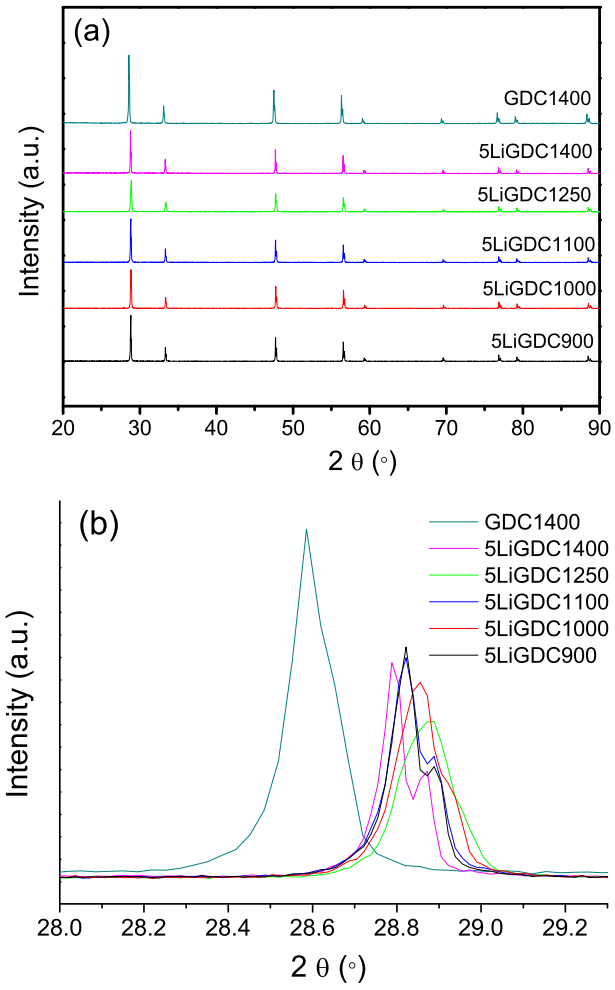

Fig. 1. The XRD of GDC1400 and 5LiGDC samples sintered at different temperatures.

height and flatness were carefully preserved while performing the XRD tests to reduce the experimental error. There were no observable secondary phases for all the 5LiGDC samples sintered at different temperatures. It is noted that there was no consistent shifting direction for the highest intensity diffraction peak (111) for 5LiGDC at different sintering temperatures, as shown in Fig. 1b. It firstly shifted to higher angle from 5LiGDC900 to 5LiGDC1000, followed by shifting back to lower angle for 5LiGDC1100, then shifted to higher angle for 5LiGDC1250 and finally shifted to lower angle for 5LiGDC1400. This is probably due to the fact that diffusion of Li into the GDC lattice and Li_2O vaporization from the GDC lattice may take place simultaneously with the increase in sintering temperature. In addition, formation of small amount of new phases/domains during the sintering process may also contribute to the lattice change.

Specifically for the lattice shrinkage effect, Li^+ (coordinate number of 8, 0.92 Å) may substitute Ce^{4+} (coordinate number of 8, 0.97Å) or Gd^{3+} (coordinate number of 8, 1.053 Å) as shown in the following reactions:

$$Li_2O \xrightarrow{CeO_2} 2Li'''_{Ce} + 3V_o^{\bullet\bullet} + O_O^{\times} \quad (1)$$

$$Li_2O \xrightarrow{Gd_2O_3} 2Li''_{Gd} + 2V_o^{\bullet\bullet} + O_O^{\times} \quad (2)$$

The doping of Li in both Gd and Ce sites is possible because it has been reported that the phase at the grain boundary core is likely to be $Gd_{0.41\pm0.04}Ce_{0.59\pm0.04}O_{1.24\pm0.17}$ due to the accumulation of Gd in sintered GDC samples without any sintering aid [18]. The backward direction of these two reactions was promoted by Li_2O vaporization from the surface of the 5LiGDC pellets while increasing the sintering temperature, which would lead to an expansion of the lattice. A series of Li–Gd–Ce–O phases [19,20] with different compositions and lattice parameters may have been formed during the sintering process. Nearly complete vaporization of Li_2O could also be expected to take place at certain high temperature. For example, the (111) peak of 5LiGDC1400 was found to be most close to that of GDC1400, indicating the most similar lattice parameter for both samples. Furthermore, the Li^+ ion doping into the GDC lattice may activate the Gd migration during the sintering process. Besides, it has been reported the existence of different Gd concentration doped CeO_2 as $Gd_xCe_{1-x}O_{2-\delta}$ with a large doping range of x from 0.1 to 0.8 [21], thus the lattice change may also happen due to the formation of such intermediate phases with different lattice constants. All these processes were finally reflected on the XRD peak shifting phenomenon observed in Fig. 1b. Due to the detection limits of XRD (~2–5% for mixed materials), the small amounts of the Li related domains and the overlapping of the background with the Li related phases, XRD is not a precise/powerful tool to examine the Li induced minor phase changes. More powerful techniques such as neutron powder diffraction (NPD), synchrotron X-ray combined with high-resolution transmission electron microscopy (HRTEM), scanning transmission electron microscopy (STEM)/electron energy loss spectroscopy (EELS) will be applied to study these structural changes in the future.

3.2. Sintering behavior

The sintering process of both GDC and 5LiGDC was studied between room temperature and 1400 °C using dilatometry. As shown in Fig. 2, the starting shrinkage temperature (Ts) was lowered from 800 °C for GDC to only 650 °C for 5LiGDC. This is mainly due to the assistance from Li_2O sintering aids. Since $LiNO_3$ decomposes to Li_2O above 600 °C, the formation of Li_2O will start to form liquid

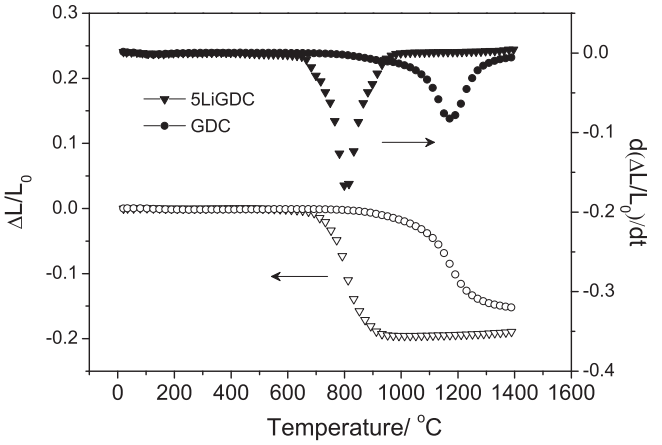

Fig. 2. Shrinkage rate (top curve) and linear shrinkage (bottom curve) as a function of the sintering temperature obtained from dilatometric experiments with increasing temperature rate of 10 °C min^{-1} for 5LiGDC and GDC.

sintering phases with Gd_2O_3 and CeO_2 (Li–Gd–Ce–O) at the same time. Table 1 showed that the temperature for the maximum shrinkage rate (Td) was also lowered to only 800 °C for 5LiGDC compared to 1175 °C for GDC. The time needed from Ts to the end of the shrinkage temperature (Te) was also reduced from 60 min for GDC to only 30 min for 5LiGDC when a heating rate of 10 °C min^{-1} was used during the dilatometry tests. Therefore, Li_2O seems to be a highly efficient sintering aid for GDC. At a sintering temperature of 950 °C, 5LiGDC already reached a linear shrinkage of 19.6% while GDC only reached 1.2%. The significant sintering promoting effect using Li_2O was closely related to the fact that the Li–Gd–Ce–O liquid phase could form at a much lower temperature. The derived free energies of formation of the mixed oxide compounds ($LiNdO_2$, $LiCeO_2$, Li_3NdO_3, Li_3CeO_3) at 923 K (650 °C) are in the range of −1424 kJ mol^{-1} to −933 kJ mol^{-1} [19], which confirmed the existing of a fast, self-motivated reaction for the Li–Nd–Ce–O system at low temperature. As both Nd and Gd were ascribed to the lanthanide series, similar results could be expected for the Li–Gd–Ce–O system in this work. Furthermore, Li_2O is much more evaporable compared to other sintering aids, such as CoO, ZnO, CuO etc [22–24]. Shown in Table 2 are the vapor pressures ($P(MO_x)$) for solid phase metal oxides (MO_x, M = Li, Fe, Co, Ni, Cu, Zn) to fully evaporate to gas phase MO_x(g) under ideal situation based on Equation (3).

$$MO_x(s) = MO_x(g) \quad (3)$$

$P(MO_x)$ can then be obtained by calculating the heterogeneous equilibrium constants (k) of Equation (3) using the function of reaction equations (HSC Chemistry 6.0 Software). Because the activity of pure solid sintering aid ($a(MO_x)$) is 1, the vapor pressure in bar is equal to k according to equation below:

$$k = P(MO_x)/a(MO_x) = P(MO_x) \quad (4)$$

Table 1
The temperature of starting shrinkage (T_s), reaching maximum shrinkage rate (T_d) and the end of the shrinkage (T_e) for GDC and 5LiGDC samples observed from sintering curve shown in Fig. 2.

	T_s (°C)	T_d (°C)	T_e (°C)
GDC	800	1175	1400
5LiGDC	650	800	950

Table 2
Calculated metal oxides–gas reaction vapor pressure (bar) of various sintering aids using the HSC Chemistry Software (version 6.0).

T (°C)	Sintering aids					
	Li_2O	Fe_2O_3	CoO	NiO	CuO	ZnO
100	8.42E-51	1.95E-65	7.96E-93	3.04E-64	6.36E-56	1.75E-58
200	4.31E-38	7.87E-50	1.21E-65	9.58E-49	3.58E-42	4.20E-44
300	7.68E-30	1.08E-39	5.16E-50	1.06E-38	3.04E-33	9.27E-35
400	4.61E-24	1.37E-32	7.07E-40	1.15E-31	5.51E-27	3.31E-28
500	8.50E-20	2.45E-27	8.88E-33	1.80E-26	2.32E-22	2.31E-23
600	1.59E-16	2.67E-23	1.56E-27	1.77E-22	8.30E-19	1.23E-19
700	6.14E-14	4.18E-20	1.66E-23	2.57E-19	5.39E-16	1.10E-16
800	7.57E-12	1.63E-17	2.57E-20	9.45E-17	1.03E-13	2.73E-14
900	3.98E-10	2.24E-15	9.87E-18	1.25E-14	7.88E-12	2.60E-12
1000	1.09E-08	1.40E-13	1.35E-15	7.57E-13	3.01E-10	1.20E-10
1100	1.79E-07	4.73E-12	8.37E-14	2.50E-11	6.66E-09	3.13E-09
1200	1.96E-06	9.77E-11	2.81E-12	5.09E-10	9.58E-08	5.20E-08
1300	1.54E-05	1.35E-09	5.76E-11	7.01E-09	8.08E-07	5.99E-07
1400	9.17E-05	1.32E-08	7.95E-10	7.03E-08	4.90E-06	5.11E-06
1500	0.000408	9.17E-08	7.92E-09	5.41E-07	0.000024	0.000034
1600	0.00142	5.11E-07	6.03E-08	3.33E-06	9.79E-05	0.000183

Li_2O showed the highest vapor pressure among all the studied metal oxides. For example, at 1000 °C, the vapor pressure reaches 1.09E-8 bar for Li_2O while it is only 1.35E-15 bar for CoO. The high vapor pressure of Li_2O ensures that Li_2O can be developed as a non-residual sintering aid. Selecting an optimized amount of Li_2O and sintering temperature is then critical to achieve this situation.

3.3. Microstructure and composition

Shown in Fig. 3 are the surface microstructures of the 5LiGDC samples sintered at different temperatures (900, 1000, 1100 and 1400 °C, respectively).

Relatively high densities (Table 3) were achieved in all the 5LiGDC sintered samples. The particle sizes on the sample surface were 0.5–0.8 μm, 0.5–1 μm, 0.4–1.1 μm, 0.5–1.4 μm and 1.2–2.5 μm for the 5LiGDC samples sintered at 900, 1000, 1100 and 1400 °C and GDC samples sintered at 1400 °C, respectively. The average grain sizes increased while increasing the sintering temperature. Seen from Fig. 3, the surface of the 5LiGDC900 and 5LiGDC1000 samples showed clearly precipitation of fine particles with diameter ~80 nm at the grain boundary regions. These may be the residues with possible Li–Gd–Ce–O phases after the sintering process. Most of them are located in the grain boundary zone, indicating that the reaction of Li_2O with Gd_2O_3 and CeO_2 took place preferentially in those regions and migrated further due to the vaporization of Li_2O on the surface of the sintered 5LiGDC pellets. Further increasing the amount of the Li_2O sintering aid to 10% mole ratio of Li^+ to GDC and lowering the sintering temperature to 850 °C (10LiGDC850) will greatly increase the amounts of these precipitation particles, and the morphology of the residues on the surface of the 10LiGDC850 sample changed obviously from single particles to larger size aggregation clusters as shown in Fig. 4. The aggregation phenomenon of the phase reaction products at lower temperature indicated the high reactivity and sinter promoting ability of Li_2O towards GDC.

Table 3
Relative density for 5LiGDC and GDC samples sintered at different temperatures.

	850 °C	900 °C	1000 °C	1100 °C	1250 °C	1400 °C
5LiGDC	89.8	99.3	98.8	97.4	97.9	97.1
GDC	61.2	63.8	69.6	73.9	77.6	95.4

Although peaks shifting phenomenon in XRD (Fig. 1) and the formation of precipitation particles for the 5LiGDC samples sintered at different temperatures (Figs. 3 and 4) were observed, there is no direct evidence to confirm the existence of Li^+ ions in the 5LiGDC sintered samples just from the XRD results alone. Secondary ion mass spectrometry (SIMS) is a surface sensitive analytical technique with exceptional sensitivity and excellent detection limits ranging from parts per million to parts per billion. As EDX could not determine the existence of the Li_2O in this study, SIMS is employed to study the surface elemental properties for the 5LiGDC sintered samples. Fig. 5 shows the SIMS surface elemental survey scan

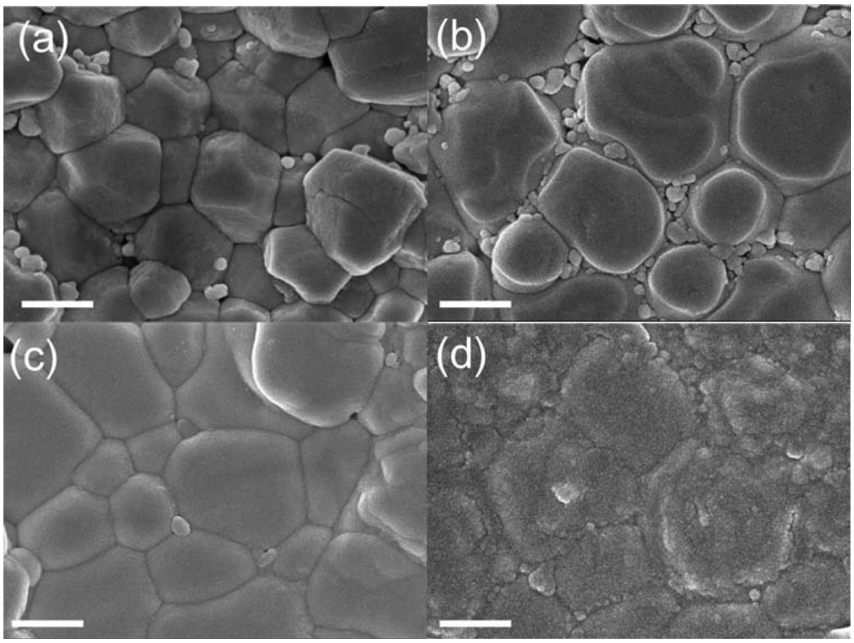

Fig. 3. SEM images of the surface of the 5LiGDC pellets sintered at 900 °C (a), 1000 °C (b), 1100 °C (c) and 1400 °C (d), respectively. All samples are not polished, and the scale bar in these images is 500 nm.

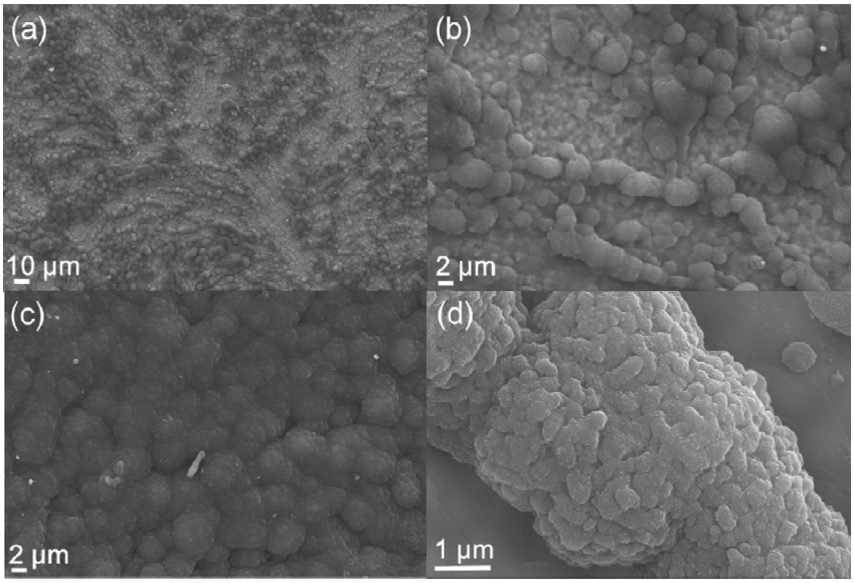

Fig. 4. SEM images of the surface from the 10LiGDC850 pellets in different magnification.

results for the 5LiGDC samples sintered at different temperatures as shown in Figs. 3 and 4. Li ion fragments (mass number (m)/charge number (z) = 6, 7), Ce ion fragments (m/z = 136, 138, 140, 142) and Gd ion fragments (m/z = 152, 154, 155, 156, 157, 158, 160) were clearly detected. These elemental fragments were further integrated respectively for each of the samples as shown in Table 4. The ratio of $Li^+/(Li^+ + Ce^+ + Gd^+)$ was found to be gradually reduced while increasing the 5LiGDC sintering temperature from 900 °C to 1400 °C. Considering the amounts of the precipitation particles in 5LiGDC also gradually reduced while increasing the sintering temperature as shown in Fig. 3, the presence of Li ion inside these precipitation particles was then expected.

The cross-section of 5LiGDC900 showed substantial amount of precipitation particles (~200–500 nm) which were mostly located in the grain boundary region as shown in Fig. 6a. In order to get more information about these small precipitation particles, TEM analysis was performed for the 5LiGDC sintered samples and EDX tests were done in the scanning transmission electron microscopy (STEM) mode with high spatial resolution (<0.1 nm). As EDX was unsuitable for the examination of light elements such as Li, the mapping results were only collected for Gd, Ce and O as shown in Fig. 6b–e. A depletion of O, Ce and Gd signals in the precipitation particles area compared with those in the bulk grains area was clearly revealed. As no other elements except for Gd and Ce were detected in the precipitation particles, the doping of Li_2O in these precipitation particles could be the most possible reason that led to the depletion phenomenon. The O signal depletion might also be ascribed to the lower oxygen ratio of Li_2O compared to CeO_2, Ce_2O_3 and Gd_2O_3, respectively.

Increase the sintering temperature up to 1000 °C and above has accelerated the vaporization of Li_2O as shown in Fig. 6g–i since no precipitation particles could be observed from the cross section of these samples. The cross section of GDC1000 (Fig. 6f) showed a porous morphology and a rather smaller grain size (~100 nm) compared to that in the 5LiGDC1000 sample (1–2 μm), clearly demonstrating the promoting effect of Li_2O towards GDC sintering. No obvious precipitation particles were observed in the cross-section of 5LiGDC1000 sample (Fig. 6g), which is different from

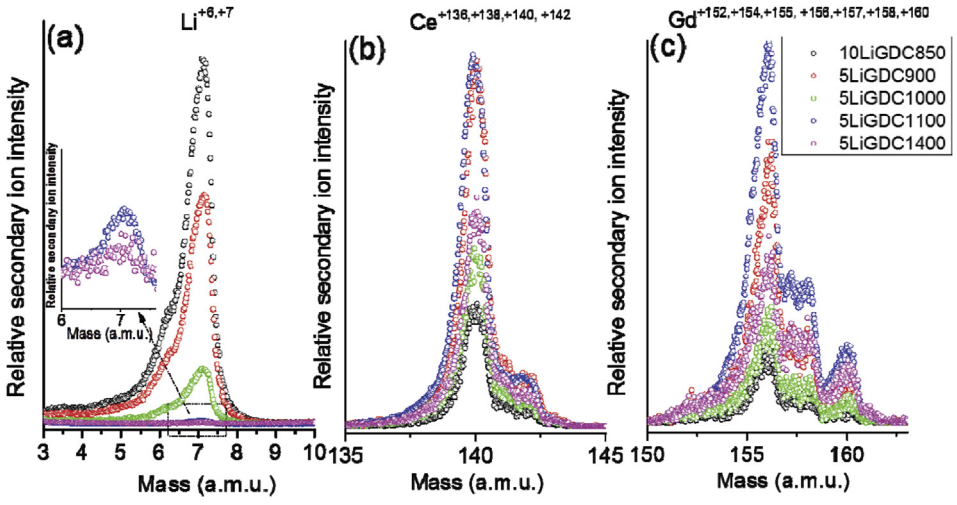

Fig. 5. Surface elements survey scan of the samples shown in Fig. 3 using secondary ion mass spectrometer (SIMS).

Table 4
Integrated SIMS signal intensity as shown in Fig. 5 for Gd, Ce, Li second ion fragments and their relative ratios for the 10LiGDC850 sample and 5LiGDC samples sintered at 900–1400 °C.

	Integrated area (a.u.)			Relative integrated area ratios			
	Gd	Ce	Li	Li/(Li + Gd + Ce)	Gd/(Li + Gd + Ce)	Li/Ce	Gd/Ce
10LiGDC850	19,683	52,134	681,232	0.904	0.0261	13.067	0.377
5LiGDC900	64,914	151,797	437,737	0.669	0.0991	2.884	0.427
5LiGDC1000	28,611	77,864	104,784	0.493	0.139	1.346	0.379
5LiGDC1100	105,333	163,335	7586	0.0275	0.381	0.0464	0.645
5LiGDC1400	57,570	97,168	–	–	0.357	–	0.592

its surface as shown in Fig. 3b. However, SIMS still detected the Li^+ fragments in the bulk of 5LiGDC1000, indicating that Li^+ may exist as nano-domains rather than large precipitation particles in the grain boundary or grain interior for the 5LiGDC1000 sample. Further increasing the Li^+ ratio to 10 mol% for GDC sintered at 1000 °C (10LiGDC1000) (inset in Fig. 6g) has resulted in a reappearance of small precipitation particles. Some small pores were generated inside the 5LiGDC samples sintered at 1100 and 1400 °C, consistent with the slightly lower relative density for both 5LiGDC1100 and 5LiGDC1400 as compared with 5LiGDC1000 samples shown in Table 3.

3.4. Electrochemical properties

3.4.1. Total conductivity

Fig. 7 showed the representative impedance spectrum for 5LiGDC1000 sample at 350 °C in air. The grain interior, grain boundary and electrode processes were separated using the equivalent circuit model as shown in the inset in Fig. 7. Three separate regions were observed in the investigated frequency range: a high frequency part corresponding to the grain interior processes (R_{GI}) (arc can be observed only at certain lower temperatures); a medium frequency arc related to the grain boundary processes (R_{GB}), and a low frequency part related to the interface processes (R_p) between the sample and electrodes. The total resistance (R_{total}) of the sample could then be obtained by the sum of R_{GI} and R_{GB}. As shown in Fig. 8, 5LiGDC900 and 5LiGDC1000 samples showed improved total conductivity compared with the GDC1400 samples. Among all the samples tested, 5LiGDC1000 samples showed the highest conductivity. At 600 °C, a total conductivity of 0.059 S cm^{-1} was achieved for 5LiGDC1000, which is much higher than that of the GDC1400 (0.019 S cm^{-1}) and among the best reported results for Gd doped ceria electrolytes [6].

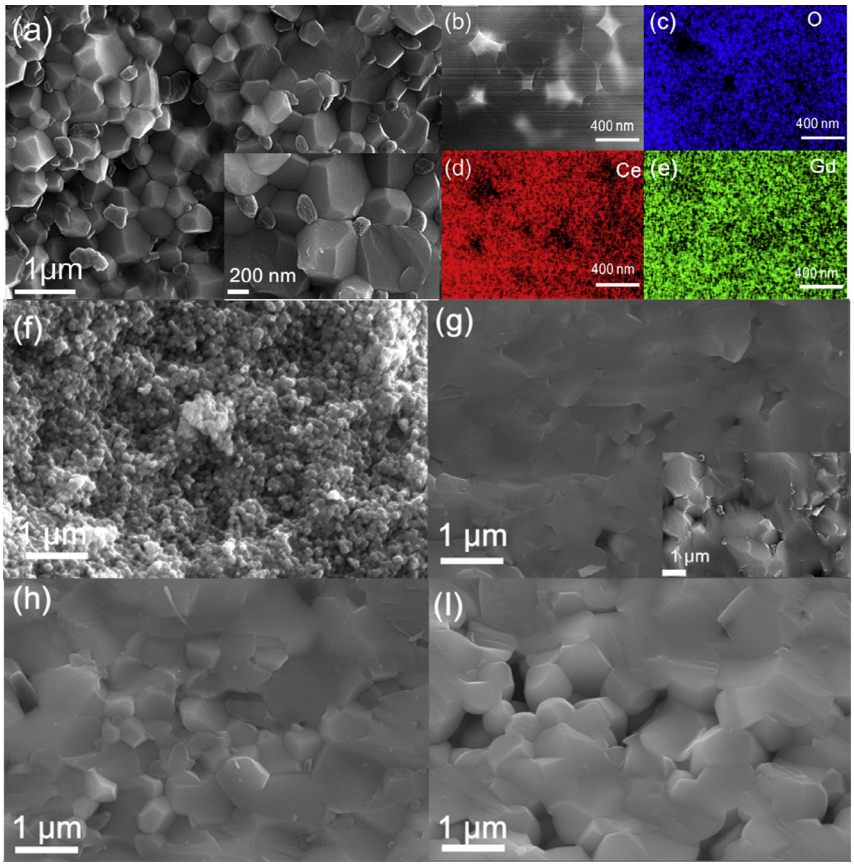

Fig. 6. SEM images of the cross-section of 5LiGDC900 (a), STEM-EDX mapping of selected area for 5LiGDC900 (b, c, d & e), and cross-section images of GDC1000 (f), 5LiGDC1000 (g) (inset is 10LiGDC1000), 5LiGDC1100 (h) and 5LiGDC1400 (i).

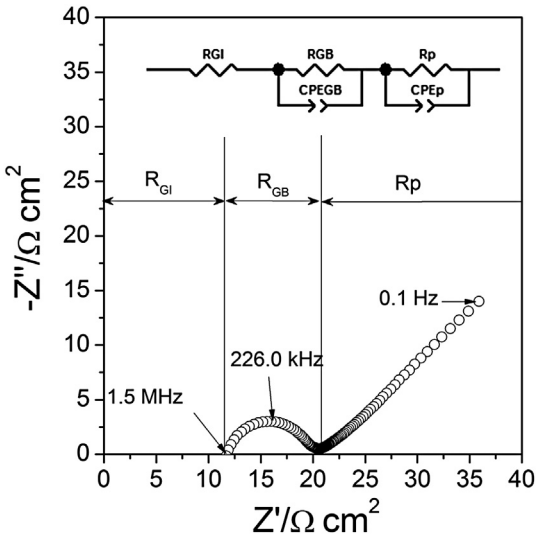

Fig. 7. Representative impedance spectrum for the 5LiGDC1000 sample at 350 °C.

3.4.2. The grain boundary conductivity

Fig. 9 shows the grain boundary conductivity of GDC1400 as well as 5LiGDC samples sintered at different temperatures. The grain boundary conductivity firstly increased from 5LiGDC900 to 5LiGDC1000. However, further increase in the sintering temperature led to a decrease in the grain boundary conductivity for 5LiGDC1100, 5LiGDC1250 and 5LiGDC1400. Furthermore, the grain boundary conductivity obtained for 5LiGDC sintered at 1100 °C and above was all very similar to that of the GDC1400 sample.

At lower sintering temperature, Li_2O may exist as Li–Gd–Ce–O precipitation phases at the grain boundary region as shown in Figs. 3, 4 and 6. The similar ionic size (with coordinate number of 8) for Li^+ (0.92 Å), Ce^{4+} (0.97Å) and Gd (1.053 Å) will result in the doping of Li^+ into CeO_2 or Gd_2O_3 with the formation of negative charges as Li'''_{Ce} and Li''_{Gd}. Both of these negative charges will compensate the positive charge (excess oxygen vacancy) in the grain boundary core [25]. This will further change the distribution of oxygen vacancy profile as schematically shown in Fig. 10. The oxygen vacancy concentration depletion effect was expected to be reduced for the 5LiGDC900 sample due to the reducing of the positive grain boundary core potential. Consequently, the over potential ($\Delta\varphi$) between the grain boundary core and the grain interior could be reduced and the grain boundary conductivity was then increased for the 5LiGDC900 sample compared with the GDC1400.

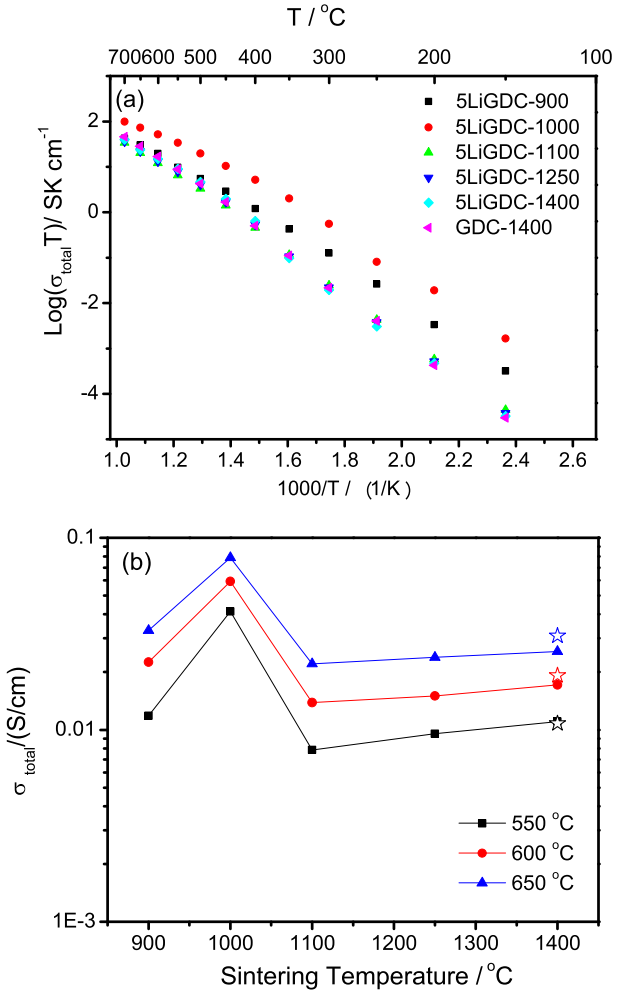

Fig. 8. The total conductivity of 5LiGDC samples sintered at different temperatures and GDC1400 (a) and sintering temperature dependence plot on total conductivity for selected temperatures for 5LiGDC sintered samples (solid) and GDC1400 (open) samples (b).

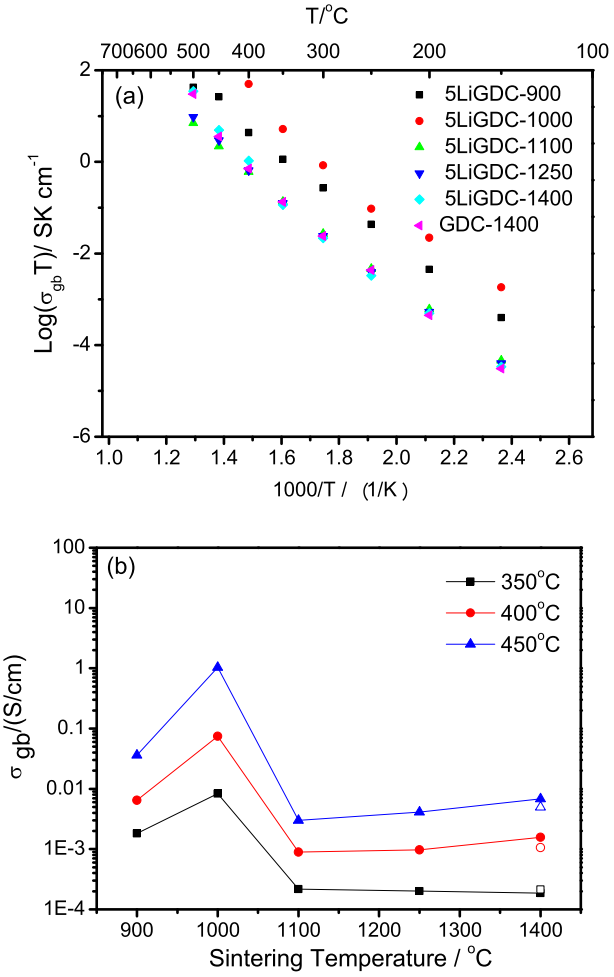

Fig. 9. The grain boundary conductivity of 5LiGDC samples sintered at different temperatures and GDC1400 (a) and sintering temperature dependence plot on grain boundary conductivity for selected temperatures for 5LiGDC sintered samples (solid) and GDC1400 (open) samples (b).

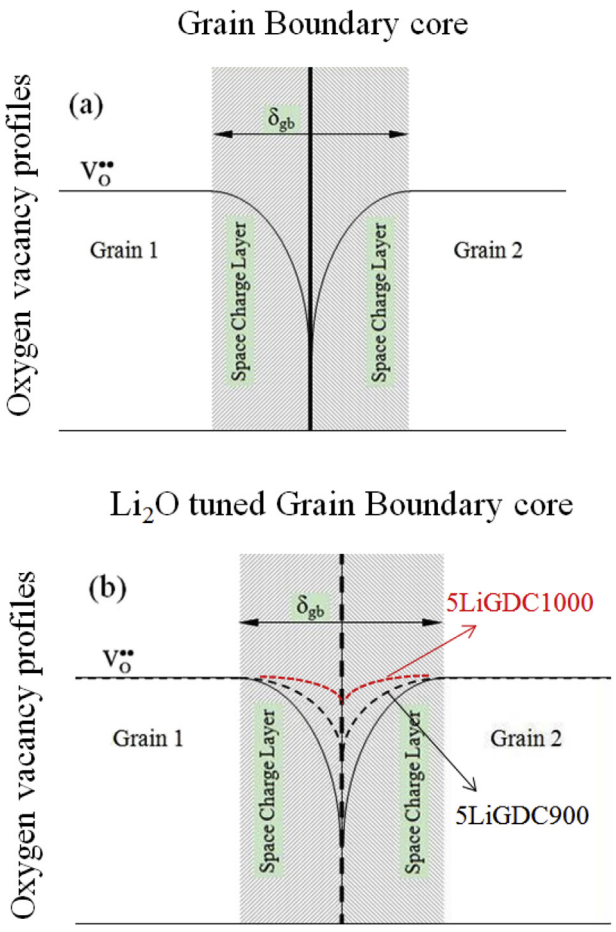

Fig. 10. Proposed oxygen vacancy profiles near the grain boundary zone based on the space charge theory for normally sintered GDC (a), as well as 5LiGDC900 and 5LiGDC1000 samples (b).

Increase the sintering temperature to 1000 °C and above will further lead to the Li containing liquid phase movements through the grain boundary promoted by the Li_2O vaporization through the sample surface. The precipitation particles enriched with Li^+ in 5LiGDC900 will compensate the decreasing Li^+ concentration in the grain boundary region until they were depleted as shown in Fig. 6g, then the effect of Gd^{3+} ion accumulation to the grain boundary region may take effect again with the further vaporization of Li_2O from the surface. At certain time, a relatively more balanced oxygen vacancy profile from the grain boundary core to the grain interior (space charge layer) may be achieved. In other words, a $\Delta\varphi$ near zero could be expected under an optimized situation (Fig. 10b). In this study, the sintering temperature of 1000 °C seems to be the optimized sintering temperature because the highest grain boundary conductivity and the smallest activation energy (Table 5) were achieved at this temperature. For example, the conductivity as high as 0.073 S cm^{-1} was reached at 400 °C for the grain boundary conductivity of 5LiGDC1000, which is one of the highest grain boundary conductivity ever achieved for doped ceria electrolyte [6].

3.4.3. The grain interior conductivity

Fig. 11 shows the grain interior conductivity of 5LiGDC samples sintered at different temperatures together with that of the GDC1400 samples. The grain interior conductivity showed maximum values for the 5LiGDC1000 sample. Meanwhile, there were little differences for the grain interior conductivity of the pellets sintered at the other temperatures, which were all similar to the grain interior conductivity of GDC1400.

Table 5
Activation energy (eV) of the total, GI and GB conductivity of the 5LiGDC samples sintered at different temperature and the GDC samples sintered at 1400 °C.

Samples	Total		GI	GB
	150–300 °C	350–700 °C	150–500 °C	150–300 °C
5LiGDC900	0.823	0.678	0.661	0.909
5LiGDC1000	0.799	0.557	0.542	0.826
5LiGDC1100	0.886	0.796	0.684	0.883
5LiGDC1250	0.894	0.776	0.689	0.884
5LiGDC1400	0.897	0.755	0.701	0.889
GDC-1400	0.929	0.838	0.705	0.931

The grain interior conductivity was believed mainly influenced by the type of doping ions, the doping concentration and the nano domain structure [26–29]. If Li^+ was doped into the CeO_2 lattice in the grain interior as shown in Equation (1), more oxygen vacancy would be created to maintain charge neutrality. Consequently, the grain interior conductivity was expected to increase due to the increasing of the oxygen vacancy concentration. On the other side, it was reported that the conductivity of $LiCeO_2$ could be as high as 1.86×10^{-3} S cm^{-1} at 420 °C [20], which is lower than the grain

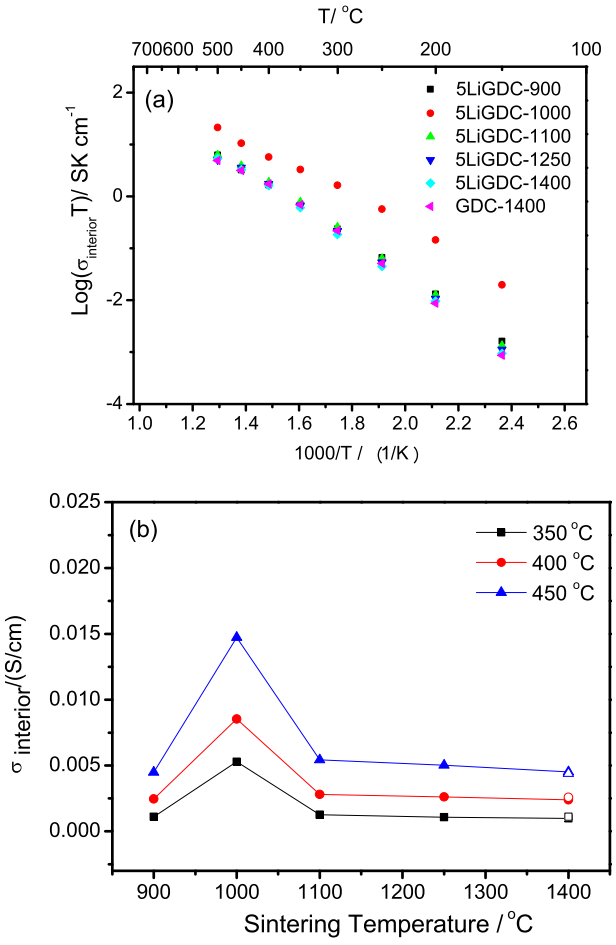

Fig. 11. The grain interior conductivity of 5LiGDC samples sintered at different temperatures and GDC1400 (a) and sintering temperature dependence plot on grain interior conductivity for selected temperatures for 5LiGDC (solid) and GDC1400 (open) samples (b).

interior conductivity of 5LiGDC900 (2.46×10^{-3} S cm^{-1} at 400 °C). Consequently, the precipitation Li–Gd–Ce–O phases in 5LiGDC900 may also be conductive and contribute to the total grain interior conductivity. Finally, the oxygen vacancy ordering due to the doping of Li^+ may also happen inside the grain interior of 5LiGDC900, which will further lower the ionic conductivity [29]. These synergistic effects will all take influence on the final grain interior conductivity of 5LiGDC900, which showed no obvious improvement compared with that of the GDC1400 sample.

Increasing the sintering temperature to 1000 °C, however, has led to an obvious increase of the grain interior conductivity and a decrease of the grain interior activation energy (Table 5) for 5LiGDC1000. As shown in Fig. 6g, no secondary precipitation particles were observed in the grain interior of 5LiGDC1000 samples. Therefore, the significant improvement of grain interior conductivity of 5LiGDC1000 compared with that of the 5LiGDC900 samples may be partially due to the disappearance of these precipitation particles as a result of the vaporization of Li_2O. It has been reported that the highest grain interior conductivity for Gd-doped ceria (conventionally sintered without adding the sintering aid) was achieved using 10 mol% ratio of Gd doped ceria (GDC10) [30]. As GDC10 was used as the starting composition in this study, there will be no expected improvement in conductivity while simply considering the change of Gd^{3+} ion concentration in GDC. Therefore, the higher grain interior conductivity of 5LiGDC1000 compared with the GDC1400 may be closely related to the Li–Gd–Ce–O phases. These Li–Gd–Ce–O phases may become a new type of nano domains with higher conductivity in the grain interior of 5LiGDC1000 during the sintering processes.

Further increasing the sintering temperature to 1100 °C and above has led to a decrease of the grain interior conductivity of the sintered 5LiGDC samples to a similar value to that of GDC1400. Furthermore, the activation energy of the GI/GB/Total conductivity all becomes similar to that of the GDC1400 sample (Table 5). Based on the SIMS results, Li_2O have mostly vaporized at 1100 °C, and the sintering process has started to become a normal sintering process without the addition of the sintering aid. Consequently, Gd^{3+} ions accumulation effect accompanied by the space charge effect [25] is expected to be enhanced by increasing the sintering temperature to 1100 °C and above.

4. Conclusions

Li_2O can be used as an efficient sintering aid for GDC, and it has found that the best condition for achieving the highest GDC conductivity is using Li_2O concentration with 5% mol ratio of Li^+ ion to GDC at the sintering temperature of 1000 °C. At 600 °C, a total conductivity of 0.059 S cm^{-1} has been achieved for 5LiGDC1000. The Li_2O promoting effect on the sintering processes and electrical properties such as grain interior and grain boundary conductivity have been analyzed. The residue elements of the sintered samples were analyzed using SIMS and possible sintering mechanism has been proposed. Formation of Li–Gd–Ce–O phases during the sintering process may have changed the elemental distribution and structure both near the grain boundary region and inside the grain interior, leading to the reconstruction of the grain boundary and grain interior of the sintered 5LiGDC samples.

Acknowledgment

We're grateful to the financial support from the US National Science Foundation (DMR-1210792), National Basic Research Program of China (973 Program, 2012CB215400) and NSFC–NSF China–US international Cooperation Project (51261120378). TEM work has been carried out at the Center for Functional Nanomaterials, Brookhaven National Laboratory, which is supported by the U.S. Department of Energy, Office of Basic Energy Sciences, under Contract No. DE-AC02-98CH10886.

References

[1] N.Q. Minh, J. Am. Ceram. Soc. 76 (1993) 563–588.
[2] Z.P. Shao, S.M. Haile, Nature 431 (2004) 170–173.
[3] M. Han, X. Tang, H. Yin, S. Peng, J. Power Sources 165 (2007) 757–763.
[4] E.D. Wachsman, K.T. Lee, Science 334 (2011) 935–939.
[5] K. Eguchi, T. Setoguchi, T. Inoue, H. Arai, Solid State Ionics 52 (1992) 165–172.
[6] B.C.H. Steele, Solid State Ionics 129 (2000) 95–110.
[7] C. Xia, M. Liu, Solid State Ionics 144 (2001) 249–255.
[8] Y.J. Leng, S.H. Chan, S.P. Jiang, K.A. Khor, Solid State Ionics 170 (2004) 9–15.
[9] K. Maca, J. Cihlar, K. Castkova, O. Zmeskal, H. Hadraba, J. Eur. Ceram. Soc. 27 (2007) 4345–4348.
[10] A.I.Y. Tok, L.H. Luo, F.Y.C. Boey, Mater. Sci. Eng. A 383 (2004) 229–234.
[11] Y.D. Zhen, A.I.Y. Tok, S.P. Jiang, F.Y.C. Boey, J. Power Sources 178 (2008) 69–74.
[12] Z. Liu, D. Ding, M. Liu, X. Li, W. Sun, C. Xia, M. Liu, J. Power Sources 229 (2013) 277–284.
[13] E. Jud, C.B. Huwiler, L.J. Gauckler, J. Am. Ceram. Soc. 88 (2005) 3013–3019.
[14] D. Pérez-Coll, P. Núñez, J.C.C. Abrantes, D.P. Fagg, V.V. Kharton, J.R. Frade, Solid State Ionics 176 (2005) 2799–2805.
[15] M. Han, Z. Liu, S. Zhou, L. Yu, J. Mater. Sci. Technol. 27 (2011) 460–464.
[16] J.D. Nicholas, L.C. De Jonghe, Solid State Ionics 178 (2007) 1187–1194.
[17] M.H.S. Zhou, Z. Liu, Z. Lei, L. Yu, S. Peng, China Patent, ZL 200910092906.X.
[18] Y.Y. Lei, Y. Ito, N.D. Browning, T.J. Mazanec, J. Am. Ceram. Soc. 85 (2002) 2359–2363.
[19] K.V. Gourishankar, G.K. Johnson, I. Johnson, Metall. Mater. Tran. B 28 (1997) 1103–1110.
[20] M. Prabu, S. Selvasekarapandian, A.R. Kulkarni, G. Hirankumar, C. Sanjeeviraja, J. Rare Earths 28 (2010) 435–438.
[21] V. Grover, S.N. Achary, A.K. Tyagi, J. Appl. Crystallogr. 36 (2003) 1082–1084.
[22] C. Kleinlogel, L.J. Gauckler, Adv. Mater. 13 (2001) 1081–1085.
[23] S.W. Tao, J.T.S. Irvine, Adv. Mater. 18 (2006) 1581–1584.
[24] K. Reddy, K. Karan, J. Electroceram. 15 (2005) 45–56.
[25] X. Guo, R. Waser, Prog. Mater. Sci. 51 (2006) 151–210.
[26] X. Guo, Z. Zhang, Acta Mater. 51 (2003) 2539–2547.
[27] H. Inaba, H. Tagawa, Solid State Ionics 83 (1996) 1–16.
[28] M. Mogensen, N.M. Sammes, G.A. Tompsett, Solid State Ionics 129 (2000) 63–94.
[29] D.R. Ou, T. Mori, F. Ye, T. Kobayashi, J. Zou, G. Auchterlonie, J. Drennan, Appl. Phys. Lett. 89 (2006).
[30] H.J. Avila-Paredes, K. Choi, C.-T. Chen, S. Kim, J. Mater. Chem. 19 (2009) 4837–4842.